Reactive Dynamics for $Zn(^3P) + H_2/D_2/HD \rightarrow ZnH/ZnD + H/D$: Rotational Populations in ZnH/ZnD Products

Michael R. Salazar and Jack Simons
Henry Eyring Center for Theoretical Chemistry
Chemistry Department
University of Utah
Salt Lake City, Utah 84112

Abstract:

Using *ab initio* multiconfigurational potential energy surfaces pertinent to the reaction $Zn(^3P) + H_2$ ---> $ZnH(^2\Sigma) + H$ and local surface tessellation and interpolation methods developed earlier, we carried out classical trajectory simulations of the title reactions, running large ensembles of trajectories with initial conditions representative of full-collision experiments. Then, using binning techniques, the ZnH/ZnD vibrational and rotational populations have been extracted. Our simulation results duplicate certain unexpected findings noted in experiments of Breckendrige *et al.* Specifically, it is observed that the rotational profiles found for ZnH produced from H_2 or from HD are nearly identical, as are the ZnD populations obtained in reactions with D_2 or HD. By interrogating the progress of reactive trajectories, we have been able to identify the origin of (much of) the rotational angular momentum in the ZnH/ZnD products which then allows us to put forth a physical model which, we believe, explains the unexpected ZnH/ZnD isotope effects in the product rotational profiles.

I. INTRODUCTION

A. The Experimental Findings and the Unexpected Isotope Effects

In the full-collision, gas-phase reactions of Zn (4s4p, ^3P_J) atoms with hydrogen molecules:

$$Zn(^3P) + H_2 \text{ ---> } ZnH(^2\Sigma) + H \qquad (1)$$

$$Zn(^3P) + HD \text{ ---> } ZnH(^2\Sigma) + D \qquad (2)$$

$$Zn(^3P) + HD \text{ ---> } ZnD(^2\Sigma) + H \qquad (3)$$

$$Zn(^3P) + D_2 \text{ ---> } ZnD(^2\Sigma) + D, \qquad (4)$$

which are electronically (i.e., ignoring vibrational zero point energies) exothermic by ca. 0.25 eV, Breckenridge *et al*. noticed that, within the error of the experiment, reactions (1) and (2) produced nearly identical ZnH product rotational and vibrational distributions.[1,2] For example, as shown in Fig. 1a, the ZnH rotational populations obtained in reaction (1) are very close to the ZnH populations realized in reaction (2). The v=0 and v=1 vibrational population ratios are also nearly the same in the two reactions. Analogous results were also observed in the ZnD product's rotational and vibrational distributions for reactions (3) and (4), which are shown in Fig. 1b. Moreover, in reactions of other s^1p^1 atoms: Mg(3s3p, $^1P_1$)[3], Cd(5s5p, $^3P_1$)[4], and (in the v=0 product of) Hg(6s6p, $^3P_1$)[5] with the hydrogen isotopes, similar results have also been observed. These findings are unexpected because the energy release in reactions (1) and (2) are not identical (due to significant zero-point energies) nor are they the same for (3) and (4). Moreover, there seems to be no (or little) dependence on the mass of the exiting atom (i.e., D would be expected to carry away different energy and momentum than H). The question to be addressed is <u>why</u> these patterns in rotational profiles occur.

In subsequent attempts to understand the origin of the rotational and vibrational population trends, and after considering the nature and symmetries of the frontier orbitals, Breckenridge *et al*. suggested that these reactions proceed via an insertion mechanism through a transition state with metal-to-H bond lengths near the diatomic equilibrium values[1,2,3] The dominance of v=0 over v=1 and v = 2 vibrational levels in the product molecules suggested the near-equilibrium metal-to-H distance at the transition state. To examine the role of exit-channel and energy surface curvature in determining the rotational populations of the products, the Breckenridge group[6] created model potentials and ran selected half-collision characteristic classical trajectories. They were able to show that, if the exit-channel potential energy surface (i.e., the surface connecting the postulated near C_{2v} inserted transition state to the H + metal hydride product) had a very specific angular anisotropy, then nearly identical rotational distributions could be obtained for reactions (1) and (2) and for (3) and (4), but they suggested that more sophisticated dynamical studies on *ab initio* surfaces should be conducted.

Although these earlier model studies suggested one possible origin for the unusual isotope effect in the product rotational populations, one is left not knowing whether anisotropy in the exit-channel surface is the dominant source of the rotational population anomaly. For this reason, we earlier undertook[7] an *ab initio* investigation into the form of the reactive energy surface for the Zn* + H_2 ==> ZnH + H reaction. The results of our determination of the surface characteristics as well as some suggestions about the fate of reactive trajectories on that surface are detailed in ref. (7). In the present work, we extend these studies to examine in detail large swarms of classical trajectories in an attempt to simulate the product rotational populations and thus, by interrogating reactive trajectories, to determine the origin of the unexpected ZnD/ZnH rotational populations.

B. Our Earlier Study of the Energy Surface for Zn(^{3}P) + H_2/D_2/HD

For the Zn* reaction, we earlier identified[7], using *ab initio* methods and reaction path following techniques, the reaction pathway that leads from Zn* + H_2 reactants, through an insertive near C_{2v} transition state and onward to ground-state ZnH ($X^2\Sigma$) + H products. We also calculated and fit, using local tessellation methods[8], the *ab initio* potential energy surface[7] (PES) for this reaction. In that earlier investigation, the $^3B_2$ entrance-channel PES, in which the Zn 4p orbital is parallel to the H-H bond axis, was proposed to be the reactive component of the ^3P Zn + H_2 surfaces. The $^3A_1$ and $^3B_1$ components are not reactive because they direct the Zn 4p orbital toward and perpendicular to the H-H bond axis, respectively. The former gives rise to a repulsive surface and the latter produces a surface that correlates to an excited (2.9 eV higher) $^2\Pi$ state of ZnH rather than to the $^2\Sigma$ ground state. Finally, in ref. (7) it was suggested that flux initially on the $^3B_2$ surface undergoes second-order Jahn-Teller coupling with a higher-lying $^3A_1$ state in which the asymmetric distortion mode of b_2 symmetry is involved, thereby distorting away from C_{2v} symmetry and proceeding onward to ground-state products on the $^3A'$ exit-channel PES. The geometries on the PES where this instability occurs defines the transition state connecting the entrance- and exit-channels. The atomic orbital basis sets, the results of calibrating our computed energies against known experimental data, and other methodological details are given in ref. (7).

C. The Present Work's Approach to the Isotope Effect Issue

Given knowledge of the reactive *ab initio* PES at ca. 1400 different geometries on the entrance-channel (i.e., for geometries connecting Zn* +H_2 to the inserted region) and at ca. 6300 geometries on the exit-channel (i.e., from the inserted region to ZnH + H), and using the local energy tessellation and interpolation methodology developed by Salazar and

Bell[8] and reviewed briefly below, it has been possible to carry out a full three-dimensional (3D) trajectory simulation of reactions (1)-(4). Specifically, by employing initial conditions reflective of the experimental conditions, we have followed many (ca. 60,000 for each reaction) classical trajectories and determined, via binning techniques, final rotational and vibrational populations of the ZnH and ZnD products. By following the courses of many such trajectories, we believe we have identified the primary sources of the products' rotational angular momentum and that we now have an understanding of the unusual ZnD/ZnH results observed in the experiments discussed above.

The outline of the remainder of this paper is as follows: Section II provides a brief overview of the PES tessellation and interpolation methodology employed for our simulations of reactions (1)-(4). Section III defines the coordinates used in the entrance- and exit-channel dynamics, describes the potential energy surfaces in both regions, how the entrance- and exit-channels are connected at the seam where second order Jahn-Teller coupling between the $^3B_2$ and $^3A_1$ surfaces is strongest. Section IV describes the initial conditions representative of the experiment performed by Breckenridge *et al.*. Contained in Section V is a sample trajectory that we found to be representative of the vast majority of reactive trajectories, our simulated rotational population data, and our analysis of the results of these simulations, including our explanation of the novel ZnD/ZnH rotational populations. Concluding the paper is Section VI.

II. REVIEW OF SURFACE TESSELLATION AND INTERPOLATION METHODS

The tessellation and interpolation methodology developed in ref. (8) has been used to generate a local piecewise description of the $^3B_2$ PES in a form especially useful for classical trajectory propagations because the forces, computed as gradients of the PES, are continuous within each local region and across neighboring regions. There are three

ingredients to this scheme: tessellation of the coordinate space used to describe the reacting species, interpolation of the energy (and its derivatives) within and across local tessellated regions, and approximation of energy gradients at the points where energies are known but analytical gradients are not available.

A. Tessellation of the Energy Surface

In the present study, we describe the entrance- and exit-channels in terms of two Jacobi coordinates, the domain of which we divide into simplices, and a third Jacobi coordinate whose influence on the PES we represent in analytical form. In two dimensions (2D) the simplices are triangles. Because a given 2D domain will admit to many different triangulations, an optimum triangulation[8] is used which attempts to minimize the number of triangles with one very small internal angle because such regions cover little area. One convenient method of facilitating this, as put forth in ref. (8), involves tessellating with barycentric coordinates and employing a so-called sphere test[9] to distinguish between competing triangulations. The barycentric coordinates (b_i) of a point x_4 , y_4 within a 2D domain are computed by solving the following set of linear equations:

$$\begin{bmatrix} 1 & 1 & 1 \\ x_1 & x_2 & x_3 \\ y_1 & y_2 & y_3 \end{bmatrix} \begin{bmatrix} b_1 \\ b_2 \\ b_3 \end{bmatrix} = \begin{bmatrix} 1 \\ x_4 \\ y_4 \end{bmatrix}, \qquad 1.$$

where the x_i's and y_i's (i =1,2,3) are the x and y coordinates of the three vertices of the triangle that make up the domain of the 2D surface. In the present study, the entrance-channel surface was divided into ca. 2600 triangles and each "slice" of the exit-channel surface (see Sec. III.B for details) was divided into ca. 1300 triangles.

B. Interpolation of the Energy Within and Across Regions

Given the tessellated domain of the PES (i.e., a set of vertex or node points $\{x_i,y_i\}$ as well as knowledge about which triangles these points lie on), along with the energies $\{E_i\}$ and gradients $\{\mathbf{g}_i\}$ at the nodes of this tessellated PES, one may interpolate the energy and gradients anywhere within the domain. This energy and gradient interpolation used in the present work is the Clough-Tocher interpolant (CT) examined in detail in ref. (8). The CT interpolant[10] expresses the energy E at a point P=x,y within any particular triangle in terms of the barycentric coordinates $\{b_i\}$ of that point determined as described above.

$$E(P) = \sum_{i+j+k+l=3} \frac{3!}{i!j!k!l!} c_{ijkl} b_1^i b_2^j b_3^k b_4^l .$$

The particular choice of the coefficients $\{c_{i,j,k,l}\}$ given in ref. (8) that defines the CT interpolant insures the continuity of the energy and its gradients within any triangle and across the boundaries of neighboring triangles and, therefore, total energy and momentum will be conserved when such an interpolant is employed.

C. Node Gradient Approximation if Analytical Gradients are not Available

Since solving the equations for the $\{c_{i,j,k,l}\}$ coefficients of the CT interpolant necessitates knowing the energies and gradients at each triangle node, and because it is quite possible that one will not have access to the *ab initio* gradients at all such points, a method for generating approximate gradients at the nodes is needed. The hyperbolic multiquadric method (MUL) has proved to be particularly useful[8] in this endeavor. The 2D MUL[11] approximates the energy E_j at a point x_j,y_j as

$$E_j\left(x_j,y_j\right) = \sum_{i=1}^{K} c_i \sqrt{d_{ji}^2\left(x_{j,i},y_{j,i}\right) + r} \qquad 2.$$

where

$$d_{ji}^2\left(x_{j,i},y_{j,i}\right) = \left(x_j - x_i\right)^2 + \left(y_j - y_i\right)^2$$

is the square of the distance from the point (x_j, y_j) where the energy is needed to the point (x_i, y_i) where the energy is known and r is a "range parameter" that controls the distance over which data influences the approximation (see ref. (8) for further discussion). The coefficients $\{c_i\}$ are determined by using Eq. (2) at the K nearest node points $\{x_k,y_k\}$ where the energies E_k are known and solving the K × K set of linear equations:

$$\begin{bmatrix} \sqrt{d_{11}^2 + r} & \cdot & \sqrt{d_{1k}^2 + r} \\ \cdot & \cdot & \cdot \\ \sqrt{d_{k1}^2 + r} & \cdot & \sqrt{d_{kk}^2 + r} \end{bmatrix} \begin{bmatrix} c_1 \\ \cdot \\ c_k \end{bmatrix} = \begin{bmatrix} E_1 \\ \cdot \\ E_k \end{bmatrix}$$

The resultant $\{c_k\}$ coefficients are then used, by differentiating Eq. (2) to obtain expressions for the desired gradients, to evaluate $\partial E/\partial x$ and $\partial E/\partial y$ at the node point (x_l,y_l) thus obtaining the needed gradient values.

III. THE REACTIVE $^3B_2$ POTENTIAL ENERGY SURFACE

A. Coordinates Used in the Entrance- and Exit-Channels

We have chosen to use the conventional Jacobi coordinates for both the entrance- and exit-channel components of our study. These coordinates on the entrance channel are the H-H' distance r, the Zn to center of mass of H-H' distance R, and the angle θ between the **r** and **R** vectors. On the exit channel, they are τ the Zn-H' distance, ρ the H to center of mass of Zn-H' distance, and φ the angle between τ and ρ. The angles α and β give the polar coordinates of **R** and **r**, respectively, and Δ and γ give the polar coordinates of τ and

ρ, resepctively. Finally, the inter-vector angles, which the potential depends on, are related to the lab-fixed polar coordinate angles by $\theta = \alpha + \beta$ and $\varphi = \Delta + \gamma$.

The time evolution of the angle coordinates α and β (or Δ and γ) are not independent since the z-component (i.e., the out of plane component) of the angular momentum,

$$L_Z = \tilde{m} R^2 \dot{\alpha} - \mu r^2 \dot{\beta} = P_\alpha - P_\beta ,$$

is a conserved quantity. Hence, it is possible to express the dynamics, for example, on the entrance-channel, in terms of a Hamiltonian (μ is the H_2 , D_2 or HD reduced mass and $\tilde{m}$ is the reduced mass of Zn relative to the diatomic):

$$H = p_R^{\,2}/2\tilde{m} + p_r^{\,2}/2\mu + (L_Z - P_\beta)^2/2\tilde{m}R^2 + P_\beta^{\,2}/2\mu r^2 + V$$

that determines the time evolution of four coordinates (R, r, α, and β) and three momenta (P_R , P_r, and P_β). Of course, a similar restriction to four coordinates and three momenta can be achieved for exit-channel dynamics.

In our simulations, we propagated trajectories in cartesian coordinates (we verified energy and angular momentum conservation) although we expressed the tessellated energy surfaces in terms of the above Jacobi coordinates. In particular, we tessellated the entrance-channel R and r coordinate space and the exit-channel ρ and φ coordinate space. The θ (entrance) and τ (exit) dependences of the potential were described by the analytical forms described in the Sec. III.B.

B. The Entrance- and Exit-Channel Potentials

1. Entrance-Channel- its Intrinsic Reaction Coordinate and the Seam Connecting to the Exit Channel

The *ab initio* PES employed for the simulations of reaction (1)-(4) is similar but not identical to the surface used in ref. (7). After examining the MP2 level surface used in our earlier work, we decided that there is reason to be concerned about the use of a single-configuration based method. Therefore, in this study, the surface was computed at the Multiconfigurational Self-Consistent Field (MCSCF) level of theory. MCSCF theory was employed to facilitate a better treatment of the two dominant electronic configurations that appear with similar amplitudes in regions where the entrance-channel and the exit-channel connect. The atomic orbital basis reported in ref. (7), which was shown there to be capable of describing reasonably well the reaction energy profile, was used in this work. However, because the overall reaction exothermicity is not adequately described at the MCSCF level of theory used here, and because we are interested in rotational and vibrational energy disposal (so we wanted a surface that reflected proper thermochemistry), we decided to (linearly) scale the MCSCF *ab initio* PESs along the intrinsic reaction coordinate (IRC) to obtain the correct 0.25 eV reaction exothermicity.

In the entrance-channel, the IRC follows the well defined and steep-sided streambed shown in Fig. 2 at large R values. As R decreases, a minimum is passed (corresponding to Zn* weakly bound to an intact H_2 molecule) after which the H-H bond begins to break (this is what necessitates the use of MCSCF methods), the IRC turns sharply to the right in Fig. 2. Proceeding toward larger r, with R remaining nearly constant, the IRC approaches the "seam" shown as a dark line in Fig. 2.

The seam is <u>not</u> simply an arbitrary line dividing what we define as entrance and exit channels. Rather, it marks the region beyond which the asymmetric stretching motion no longer has positive curvature due to second-order Jahn-Teller coupling. Beyond this

seam, trajectories no longer experience forces that act to retain both Zn-H bonds; rather, at the seam, the surface undergoes a qualitative change to one where the forces cause one Zn-H bond to spontaneously dissociate. This instability of the ZnH_2 triplet surface makes it and the subsequent dynamics on it qualitatively different than what is observed in other A + $H_2 \rightarrow$ AH + H reactions(e.g., the $O(^1D) + H_2 \rightarrow OH + H$ reaction[12] which proceeds through a similar insertive mechanishm but via the very deep well on the ground-state surface coresponding to an intact, but highly vibrationally excited, H_2O molecule).

It should be noted that the geometry in the seam region is much like Breckenridge *et al.* had speculated - the Zn-H bond length is near its equilibrium value (a bit elongated) and the complex clearly has an "inserted" shape. Moreover, the H-H bond is nearly fully broken at the seam, as evidenced by the HZnH bond angle of ca. 60°. This point will play an important role in our later interpretation which assumes that the zero-point energy contained in the H_2 , D_2 or HD molecule is released by the time the seam is reached.

As mentioned earlier, the θ-dependence of the entrance-channel surface is given by an analytical potential. In particular, we chose to represent this dependence in terms of a local quadratic form in terms of $\cos\theta$ (or, equivalently, in terms of the difference between the distances Δr_{AB} and Δr_{AC} between the Zn atom A and the two H atoms B and C):

$$V(r,R,\theta) = V^{3}B_2(r,R,\theta = \frac{\pi}{2}) + \frac{1}{4}k(R)(\Delta r_{AB} - \Delta r_{AC})^2. \qquad 3.$$

The asymmetric distortion force constant k(R), which depends strongly on location along the IRC, was obtained by carrying out *ab initio* MCSCF Hessian (i.e., analytical curvature) calculations at 40 points along the IRC of the entrance-channel. The resulting k(R) force constant data were then fit to a functional form as shown in Fig. 3.

Clearly, at large R, trajectories encounter very weak angular restoring forces consistent with nearly free rotation of the H_2 molecule. As R decreases along the IRC,

much stronger angular forces arise, with the strongest forces arising near the region in Fig. 2 where the IRC begins to turn sharply to the right. These forces are due to the attractive interaction between the Zn atom's 4p orbital and the H_2 molecule's antibonding σ_u orbital which prefer to be aligned parallel to one another. When we examine individual trajectories, these strong angular forces are observed to align the ZnH_2 complex into near C_{2v} geometries. As R decreases further (i.e., as the IRC moves to longer r and approaches the seam region shown in Fig. 2), the angular force constant falls off rapidly until, at the seam, it becomes negative, meaning that the complex no longer is stable at C_{2v} symmetry. Once the seam is crossed, k(R) goes to zero and the surface becomes unstable to loss of one H atom. From the seam onward, neither the above angle-dependent function nor the tessellated surface depicted in Fig. 2 is used to calculate the PES and its gradients. Rather, we employ new Jacobi coordinates and a PES expressed in terms of these coordinates from the seam onward to products.

2. Exit-Channel

The exit-channel IRC is shown in Fig. 4 which displays the PES at a value of τ = 1.7Å as a function of two of the Jacobi coordinates (ρ and φ). We computed MCSCF energies at a grid of points in ρ, φ space with τ held fixed at τ = 1.7 Å to generate the 2D slice through the exit-channel energy surface shown in Fig. 4. We repeated this series of calculations at 9 different τ values ranging from τ = 1. 4 Å to τ = 2.2 Å spaced by 0.10 Å. When propagating trajectories from the entrance to the exit-channel a decision must be made when the trajectory reaches the seam. This decision is which of the 2D slices to use

in determining the ρ, φ dependence of the surface. We choose that slice whose τ value (τ^0) is closest to the value of τ realized when the trajectory reaches the seam

$$V(\rho,\varphi,\tau) = V^{3A'}(\rho,\varphi,\tau = \tau^0).$$

The gradients along ρ and φ are then computed using this particular 2D surface (until time evolution of τ causes it to achieve a value closer to another slice's τ^0 value after which that sheet's 2D surface is used). The gradient of the PES along τ is approximated by taking the finite difference between the potential at (ρ,φ) for exit-channel slices having τ values slightly less than and slightly larger than the current sheet's τ^0 value:

$$\frac{\partial V}{\partial \tau} = \frac{V^{3A'}(\rho,\varphi,\tau = \tau^i) - V^{3A'}(\rho,\varphi,\tau = \tau^j)}{\tau^i - \tau^j}.$$

Because the τ-spacing between sheets is only 0.10 Å, these finite differences are found to yield reasonably smooth changes in the forces along τ as evidenced by the lack of any "jerky" behavior in plots of the time dependence of ρ, φ, and τ (see Sec. V.A for an example). Moreover, we examined graphs of $V(\rho, \varphi, \tau)$ vs τ, obtained from our 9 slices, for many asymptotic values of ρ and φ. We found they did not exhibit unusual jerks and that they resemble closely a plot of the Morse potential for an isolated ZnH diatomic molecule.

IV. INITIAL CONDITIONS FOR CLASSICAL TRAJECTORIES

A. Linear Coordinates, Momenta, and Weights

The initial distance R of the Zn atom from the center-of-mass of the hydrogenic diatomic was taken to be 4.5-5.0 Å in all trajectories (this is large enough to be in the asymptotic region). The initial relative momentum p_R (always negative to simulate a collision) of the Zn and diatomic reactant was obtained from a Maxwell-Boltzmann distribution of speeds at the experimental temperature of 350 °K, with weight of $4\pi (\tilde{m}/2\pi kT)^{3/2} v^2 \exp(-\tilde{m}v^2/2kT) \Delta v$, where v is the relative velocity along R.

The initial distance r of the hydrogen diatom was sampled over a range between the inner and outer turning points for the diatom in its v=0 vibrational level with a weighing of $|\psi_{v=0}(r)|^2 \Delta r$. The initial vibrational momentum p_r of the diatom was then determined by using the bond length r and conservation of energy:

$$p_r^2/2\mu + V_{HH}(r) = 1/2\hbar\ (k/\mu)^{1/2}.$$

Except at the turning points, both positive and negative values for p_r were selected, with a separate trajectory run for each case.

B. Angular Coordinates, Momenta, and Weights

The impact parameter b was varied from 0.0 Å to ± 1.5 Å in units of 0.3 Å with a weighting factor of $2\pi b\ db$; the maximum impact parameter was determined by examining when the reaction probability decreased sufficiently to ignore larger b values. The Zn atom's angular coordinate α was computed from $\cos\alpha = b/R$. Each b value produces $\tilde{m}\dot{R}b$ in collisional angular momentum as a contribution to the total initial angular momentum. The velocity corresponding to the angle α is computed as $\dot{\alpha} = \frac{\dot{R}b}{R^2}$.

The initial value of the hydrogen diatom's phase angle β was systematically varied from 0 to $\pi/2$ for H_2 and D_2 and from 0 to π for HD in units of 15 degrees (these limiting values of the angle β were chosen to avoid redundant simulations). The initial rotational angular velocity $d\beta/dt$ was obtained from the angular momentum of the hydrogen diatom $(\mu r^2 d\beta/dt) = J(J+1)B$ for the diatom in J=0, 1, 2 (for H_2) and J=0, 1, 2 and 3 (for HD and D_2) and was allowed to take on both positive and negative projections along the axis perpendicular to the molecular plane. The weight associated with the rotational state was proportional to $(2J+1)\exp(-BJ(J+1)/kT)$.

Although our methods for choosing initial conditions for our trajectories may not be as efficient as, for example, Monte-Carlo sampling or more sophisticated means[13] of discretizing and sampling the ranges of coordinates and momenta values, because we use so many trajectories and because they are, in principle correct, our final results can be trusted.

V. RESULTS AND EXPLANATION OF ISOTOPE EFFECTS

A. Sample Trajectory

A sample reactive trajectory for $Zn(^3P)$ colliding with H_2 on the entrance-channel potential detailed above and then moving through the seam to the exit-channel surface(s), also described above, is shown in Fig. 5. The initial conditions for this trajectory have the Zn atom colliding with the H_2 at the most probable velocity for 350 °K, with an impact parameter of 0.6Å (typical of many reactive trajectories), with the H_2 in the J=1 rotational level, and, of course, with H_2 in its v = 0 vibrational level. The outcome of this simulation produced a ZnH molecule in v=1 and in the N=6 rotational level.

Although only one trajectory is shown in Fig. 5, it displays characteristics seen in virtually all reactive trajectories that we have examined, and these characteristics weigh heavily on the explanation that we put forth for the unexpected rotational isotope effects (see Sec. V.C). Therefore, it is important to discuss some of the behavior seen in this one trajectory.

The time evolution of the H-H coordinate, r, and the relative orientation angle θ as well as that of the interfragment distance R are shown on the left side of Fig. 5. As the Zn atom begins to interact strongly with the H_2 molecule, at ca. t = 1750 a.u., the H-H bond suddenly begins to lengthen. At this time, the trajectory is starting to move from the entrance valley shown in Fig. 2 (near R = 1.8 Å, with the H-H bond still intact at r = 0.8Å) toward the seam region where movement to the exit-channel can occur (in Fig. 5, the exit-channel is accessed at ca. t = 2700 a.u.). The time evolution of $\theta=\alpha+\beta$ is characteristic of free rotation (with small $\dot{\alpha}$) until ca. t = 1100 a.u.. Beyond t=1100 a.u., $\dot{\alpha}$, which is negative, becomes large enough to reverse the sign of $\dot{\theta} = \dot{\alpha} + \dot{\beta}$. As t approaches and passes 1750 a.u. forces due to the approaching Zn atom cause θ to "lock in" at near C_{2v} geometry (i.e., $\theta \approx 270°$) and to change very little with time beyond t=2200 a.u..

Once the seam is reached, r is much longer than the equilibrium H-H bond length (so this bond is essentially fully broken) and the ZnH_2 complex has assumed a triangular "inserted" geometry as Breckenridge *et al.* postulated. Moreover, at the seam, the Zn-H distance is close to the equilibrium bond length (1.6Å) of isolated ZnH ($X^2\Sigma^+$), again as the experimentalists had suggested.

Once on the exit-channel, the interfragment distance, ρ, grows monotonically indicating that the ZnH and H undergo prompt fragmentation, while the Zn-H distance τ undergoes oscillation characteristic (at long time) of isolated ZnH vibration (n.b., $d\tau/dt$ is

positive when the exit-channel is first accessed). The time dependence of the angle φ, which, of course, is related to the relative angular momenta of the separating fragments, shows an initial positive slope ($d\varphi/dt$ relates to angular momentum) that decreases somewhat as time progresses and seems to reach a constant value at long time. We will have more to say about this angular velocity below in Sec. V.D where our model explaining the isotope effects is put forth. For now, suffice it to say that the characteristics detailed above are typical of all reactive trajectories and form much of the basis of our model.

B. Simulations' Rotational and Vibrational Population Data

Well over 200,000 trajectories were run to simulate reactions (1)-(4) using the distributions of initial conditions discussed earlier. In binning the rotational populations, we inferred an N value from the total asymptotic rotational energy[14], E_{rot}, of the product ZnH or ZnD molecule using $E_{rot} = N(N+1)\,B$, where B is the rotational constant of the diatomic. This N (non-integer) value is then rounded to the nearest integer value to permit binning of that trajectory to a particular N. We then "smoothed" this distribution (denoted P(N)) to obtain the final distributions, $\bar{P}(N)$, used in subsequent analysis. The particular smoothing expression that we used involves defining $\bar{P}(N) = 1/2\,[P(N) + 1/2\{P(N-1) + P(N+1)\}]$.

Figs. 6-7 show the distributions of rotational populations for products in the v=0 and v=1 states of ZnH and Figs. 8-9 give the distributions in the v=0, and v=1 states of ZnD, when reactions (1)-(4) are simulated (v = 2 ZnD data are not shown because of poor statistics). As was done for the experimental populations shown in Figs. 1, the distributions were normalized so that the area under each distribution is unity.

1. ZnH from H_2 and from HD

As seen in Fig. 6, the **v=0 ZnH** rotational distributions from H_2 and from HD have "cut off values" (19-20$\hbar$) (i.e., maximum N values that have any significant population) that are very nearly the same and close to the experimental values (19$\hbar$) of Figs. 1. This indicates that the overall exothermicity, which plays a central role in determining these cut offs, is correctly described in our simulations. Moreover, the maxima in the simulations' probability distributions are similar for ZnH produced either from H_2 or from HD, in line with the (surprising) experimental finding. This maximum of 8$\hbar$ is 3$\hbar$ lower than the peak in the experimental plots (11$\hbar$) shown in Figs. 1.

The **v=1 ZnH** results shown in Fig. 7 have a cut off in both the H_2 and HD simulations near 18$\hbar$ which is in excellent agreement with the experimental result. The peak in the v=1 ZnH rotational distribution lies at ca. 7$\hbar$, which again is ca. 3$\hbar$ below the experimental result.

2. ZnD from D_2 and from HD

The **v=0 ZnD** simulation results shown in Fig. 8 show cut off values of ca. 25-26$\hbar$ and 26-29$\hbar$ from D_2 and HD, respectively, while the experimental cut off for both occurs at 26$\hbar$. The peaks in the simulations' distributions are difficult to evaluate due to scatter in the data; estimates ranging from 10$\hbar$ to 12$\hbar$ would be reasonable the ZnD, while the experimental v=0 ZnD data show a peak at 15$\hbar$. The simulations' HD distribution seems to be a bit wider than the D_2 counterpart.

Fig. 9 shows the **v=1 ZnD** simulation results which display cut offs at ca. 23-25$\hbar$ for both the ZnD product from D_2 and HD, while the experimental results show a cut off at

$23\hbar$. The peaks in the distributions from the simulations lie between 6 and $10\hbar$ while the experimental results show a peak at 11 or $12\hbar$.

C. Origins of Product Angular Momentum

Because our simulated rotational profiles seem to reproduce to a reasonable extent (but not quantitatively) the experimentally observed features that ZnH populations produced in reactions with H_2 and with HD are nearly identical, as are ZnD populations from D_2 and from HD, we decided to interrogate our reactive trajectories in hopes of uncovering the physical origin of this result. Before discussing the result of our interrogations, let us briefly examine various possible sources of product ZnH or ZnD rotational angular momentum. Because total angular momentum is conserved, any found in the ZnH or ZnD products must combine with that taken away by the departing H or D atom (i.e., it's angular momentum relative to the center of mass of the nascent diatomic) to balance the angular momentum initially present in the collision.

1. Rotational, collisional, and electronic angular momenta

All trajectories begin with angular momentum of three types. The H_2, HD, or D_2 molecules have rotational angular momentum, but, due to Boltzmann populations at the temperature of the experiment, only J = 0 through 3 are significantly populated. So, at most 3 units of angular momentum come from this source. The Zn* atom, which has one unit of electronic angular momentum in its P state, collides with the hydrogen molecule over a distribution of impact parameters (b) and with a distribution of collision speeds (v) characteristic of 350 °K. Using a speed determined at the maximum of the Maxwellian distribution and an impact parameter (b= 0.75 Å) equal to that for which many trajectories

reacted (equal to one-half of b_{max}), we compute collisional angular momenta of ca. $4\hbar$ for H_2, $5\hbar$ for HD, and $6\hbar$ for D_2.

2. Even the most constructive additions of these angular momenta is not enough

These angular momenta can combine in either a constructive or destructive sense (e.g., if the H_2 is rotating clockwise, the collisional angular momentum may be clockwise or counter clockwise) to produce the total initial angular momentum. At most (i.e., for the most constructive case but using the most probable collisional angular momenta), one obtains total initial angular momenta of $7\hbar$ for H_2, $9\hbar$ for HD, and $10\hbar$ for D_2, all of which are substantially below the angular momenta experimentally observed for the ZnH or ZnD products (see Fig. 1). Hence, there must be another source of product angular momentum.

3. All of the initial angular momentum can not end up in the ZnH product's rotation

What is the fate of the initial angular momentum and what other sources exist? We know from our analysis of reactive trajectories that, in the seam region of the entrance-channel PES, the ZnH_2 moiety is "locked into" a near C_{2v} geometry. This implies that all of the ca. 7-$10\hbar$ of initial angular momentum has evolved into rotational angular momentum of the entire ZnH_2 species. If, after crossing the seam, the rotating ZnH_2 suddenly breaks apart into an intact ZnH molecule and a departing H atom, only one-half of the total angular momentum would be carried off in rotation of the ZnH diatom (because all three atoms rotate about the molecular center-of-mass with identical angular velocities). In the ZnHD case, only one-third of the total angular momentum would depart with a nascent ZnH molecule, while two-thirds would appear if ZnD is formed. It is experimentally observed that ZnH produced from ZnH_2 and from ZnHD has nearly identical rotational

angular momenta, and that ZnH produced from HD does not have only $\frac{1/3}{2/3} = \frac{1}{2}$ the rotational angular momentum of ZnD from HD. Moreover, as noted in the preceeding paragraph, even all of the angular momentum of the rotating ZnH_2 complex is too small to account for the angular momentum observed in the ZnH or ZnD products. Hence, there must be more to this story than product-deposition of initial collisional-plus-diatom angular momentum.

D. Physical Model for (the rest of) the Products' Angular Momentum

In search of other sources of product angular momentum, we examined the nature of numerous reactive trajectories as they crossed the seam in the entrance-channel PES and observed that:

1. most of the internal motion (i.e., velocity excluding overall rotation) in the ZnHH complex resides in dr/dt and dr/dt is positive (due largely to release of the zero-point vibrational energy in the H-H bond that is nearly fully broken when the seam is reached),
2. dR/dt is small and can be positive or negative, and
3. $d\theta/dt$ is small (this is reflective of the HH rotational motion being "locked in").

Using the internal geometry of the collision complex in the seam region (e.g., R = 1.6 Å; r = 2.4 Å) and drawing velocity vectors that characterize large dr/dt, we were able to identify a potential source of significant angular momentum in the diatomic product (see Fig. 10).

1. Release of Zero-Point Vibrational Energy

Notice that the departing H atom (the one on the right in Fig. 10) has a large component of its velocity along ρ consistent with prompt dissociation of the ZnH + H

fragments, and that its component perpendicular to ρ is such that the angle φ increases (i.e., $d\varphi/dt$ is positive). Also, note that the H atom involved in forming ZnH (the one on the left) has a velocity vector with a large component ($v_{H,per} = v_H \sin\chi$) perpendicular to the Zn-H axis whose length is τ. This velocity vector can generate angular momentum equal to $\mu_{ZnH}\ \tau\ v_{H,per}$. Thus, our proposal for the source of the additional angular momentum in the diatomic products is this velocity of the separating H atoms that is converted both into relative velocity of separation (for the departing H) and ZnH rotation (for the other H).

Continuing to examine the above model, we speculate that the source of most of the velocity dr/dt is the release of zero-point energy in the H-H molecule which, upon reaching the seam region, has it's bond nearly broken. If this is the case, we should have $dr/dt = (2\Delta E/\mu)^{1/2}$ with $\Delta E = 1/2\hbar\ (k/\mu)^{1/2}$, the zero-point energy. So, dr/dt should be proportional to $\mu^{-3/4}$. In the homonuclear cases, H_2 and D_2, the velocity of the H or D atom is $\frac{1}{2}\frac{dr}{dt}$, but in the HD case, the H atom's velocity is $\frac{2}{3}\frac{dr}{dt}$ and the D atom's velocity is $\frac{1}{3}\frac{dr}{dt}$. Combining these facts, we can express hydrogen isotopic mass dependence of the rotational angular momentum in terms of the equation:

$$L_z = \mu_{Zn,H/D}\ \tau\ v_{H/D} \sin\chi\ .$$

Recalling that $v_{H/D}$ is proportional to $(\mu_{HH/HD/DD})^{-3/4}$ and that v is $\frac{1}{2}\frac{dr}{dt}$ for HH and for DD but involves $\frac{1}{3}\frac{dr}{dt}$ and $\frac{2}{3}\frac{dr}{dt}$ for HD, we can compute the rotational angular momenta appropriate to the four isotopic cases. These predictions (which, of course provide a single value for each isotopic case, and, thus, relate most likely to the peaks in the distributions) are summarized in Table I.

The physical model in which zero-point energy of the H_2, D_2, or HD molecule is converted into relative motion (outward) in the r coordinate which then generates torque on the newly formed ZnH or ZnD bond axis to generate (a major portion of) the products' rotational angular momentum suggests, according to Table I, that the ZnH rotational angular momentum should be nearly the same (with a ratio of 0.84/0.90 = 0.93) when H_2 or HD is the reactant. Likewise, the rotational angular momentum of ZnD from HD and from D_2 should be nearly the same (with a ratio of 0.90/1.0 = 0.90). In both cases, the case in which D is the departing atom should produce the (slightly) hotter rotational profile in the diatomic.

2. Combining All Sources of Angular Momentum

In summary, the following major generators of angular momentum have been identified:

a. the collisional angular momentum and the $1\hbar$ contributed by the Zn* atom (5-$7\hbar$),

b. the initial rotational angular momentum of the hydrogenic diatomic (0-$3\hbar$),

c. and the release of zero-point energy into torque of the nascent ZnH or ZnD (13-$15\hbar$).

All of these sources of angular momentum can add constructively or destructively. For example, if the ZnHH complex shown in Fig.10 were rotating clockwise with $7\hbar$ of angular momentum (of which $3.5\hbar$ would end up in the nascent ZnH), release of zero-point energy would increase to ca. $16.5\hbar$ (= $3.5\hbar$ + $13\hbar$) the rotational angular momentum in the ZnH fragment. In contrast, if the ZnHH complex were rotating counter clockwise with $7\hbar$ of angular momentum, release of zero-point energy would produce ZnH rotating with $13\hbar$ - $3.5\hbar$ = $10.5\hbar$ of angular momentum.

The overall result of combining these three sources of angular momentum is

a. a distribution of angular momenta in the ("locked") ZnHH (or ZnDD or ZnHD) complex of ca. $2\hbar$ to $10\hbar$ of which 1/2, 1/3 or 2/3 is available to the ZnH or ZnD product molecule (so, only $1\hbar$ to $7\hbar$ of product rotation arises from this source), and

b. an additional amount of product molecule angular momentum of ca. $13\hbar$ to $15\hbar$ generated by release of zero-point energy, which can combine constructively or destructively with the angular momentum of source a.

The net result is a wide distribution of rotational energies in the ZnH or ZnD products, but a distribution that has a major contribution from the angular momentum generated by release of zero-point energy.

3. Computer Simulation Test of the Zero-Point Energy Release Model

To further test the primary hypotheses on which the above model is based, we examined, for the same ensemble of reactive trajectories used to generate the rotational profiles shown earlier, the angular momentum of the ZnH and ZnD at the moment the trajectory first accesses the exit-channel PES (i.e., once the seam shown in Fig. 2 is first crossed). Figs. 11and 12 show these distributions for ZnH and ZnD, respectively. These distributions are not vibrational-state resolved. That is, they include contributions from all vibrational states and, as such, should be compared to the sums of Figs. 6-7 and Figs. 8-9 for ZnH and ZnD, respectively.

The data shown in Figs. 11-12 describe the rotational level the diatomic would occupy if all forces due to the presence of the departing H or D atom were suddenly removed once the exit-channel is accessed. The differences between the distributions of rotational angular momentum obtained in this limiting-case and in our full simulations are due to the influence of the departing atom on the nascent diatomic.

The data depicted in Figs. 11 and 12 show that the nascent ZnH rotational angular momentum distributions from Zn reacting with H_2 and with HD have very similar onsets

(ca. $5\hbar$), cut off values (ca. 25-26$\hbar$) and peak values (16-17$\hbar$), but, consistent with the model put forth above, the distribution from HD is slightly hotter. Similarly, the nascent ZnD rotational distributions for product produced from Zn reacting with D_2 and HD have nearly identical onsets (ca. $6\hbar$), cut offs ($34\hbar$) and peak values (ca. 15-17$\hbar$), but again with the products formed from D_2 being slightly hotter.

When these nascent distributions are compared with the final rotational distributions obtained in our simulations, significant differences are noted, but it is important to stress that the populations shown in Figs. 11-12 suggest the key (unexpected) characteristic of the experimental data and of our full simulations - that the rotational populations of ZnH from H_2 and from HD are (nearly) the same and the distributions of ZnD from D_2 and from HD are (nearly) the same.

The primary differences between the distributions of nascent ZnH or ZnD and of experimental (or simulated) ZnH or ZnD are:

1. that the cut offs shift to lower values (by ca. $6\hbar$) as trajectories move from the seam region to form products.
2. that the peak values also shift to lower values;
3. that the onsets shift all the way to $0\hbar$ for both ZnD and ZnH.

The source of shifting (downward) in the cut offs and peaks as well as the broadening in the rotational profiles when moving from the seam region to the final products is the curvature or angle-dependence of the exit-channel PES, as shown in Fig. 4. Trajectories passing through the seam have

I. significant velocities along ρ (as discussed above) that causes prompt fragmentation, and

II. the nascent ZnH and the departing H have <u>relative</u> angular momenta of opposite signs (i.e., the Zn-H bond moves in a sense opposite to the movement of the departing H atom although, as noted earlier, all three atoms are also rotating as a unit with all three atoms

having the same angular velocities because of the initial collisional and diatomic angular momentum).

Because of the fact II., trajectories exiting the seam region and moving toward fragmentation possess positive $d\varphi/dt$ and hence move toward larger φ values on the exit-channel PES (see Fig. 4). As they move to larger φ, they encounter forces that drive them away from even higher φ (i.e., de-torquing forces that keep the H-Zn-H moiety away from collinear geometries). These forces thus reduce (and broaden) the angular momentum in the product molecules, thus accounting for the differences between the rotational profiles of Figs. 11-12 and the experimental data.

VI. CONCLUSIONS

Using classical trajectory simulations on an *ab initio* multiconfigurational potential energy surface for the $^3B_2$ (or $^3A'$) state of the $Zn^*(^3P) + H_2 \rightarrow ZnH\ (^2\Sigma) + H$ reaction and a local tessellation and interpolation scheme, we were able to replicate much of the unusual results observed in the experimental ZnH and ZnD product rotational populations. Subsequent interrogation of reactive trajectories suggests that <u>much</u> of the product rotational angular momentum is generated by release of the H_2, D_2, or HD zero-point energy near the triangular transition state, but significant contributions also arise from initial rotation of the hydrogenic diatom and collisional angular momentum. When the zero-point energy is released, outward velocity along the H-H (or D-D or H-D) axis both propels the departing hydrogenic atom outward and generates torque on the nascent Zn-H (or Zn-D) bond thereby producing rotational angular momentum. As trajectories move further on the exit channel surface, some of the angular momentum thereby generated is lost due to forces

that act to push the departing atom and the nascent diatomic back toward triangular geometries.

A simple model, based on consuming all of the initial zero-point energy to produce rotation in the product diatomic predicts that the ZnH rotational angular momentum when H_2 is the reactant should be nearly the same as when HD is used (and that the ZnD angular momentum from D_2 and from HD should be nearly identical). Inclusions of initial collisional-plus-diatomic rotational angular momentum from these broadens and shifts the product-molecule rotational population profiles.

Acknowledgements:

This work was supported by NSF Grant CHE 9618904. We are very grateful to our colleague W. H. Breckenridge for sparking our interest in this problem and for many enlightening discussions.

References:

1. W. H. Breckenridge and J. Wang, *Chem. Phys. Letters*, **123**, 17 (1986).

2. W. H. Breckenridge and J. Wang, *J. Chem. Phys.*, **87**, 2630 (1987).

3. W. H. Breckenridge and J. Wang, *Chem. Phys. Letters*, **137**, 195 (1987).

4. W. H. Breckenridge, H. Umemoto and J. Wang, *Chem. Phys. Letters*, **123**, 23 (1986).

5. N. Bras, J. Buteaux, J.C. Jeannet and D. Perrin, *J. Chem. Phys.*, **85**, 280 (1986).

6. W. H. Breckenridge and J. Wang, *Chem. Phys. Letters*, **139**, 28 (1987).

7. M. R. Salazar and J. Simons, *J. Chem. Phys.*, **105**, 10919 (1996).

8. M. R. Salazar and R. L. Bell, *J. Comp. Chem.*, in press.

9. C. L. Lawson, *Comput. Aided Geom. Design*, **3**, 231 (1986).

10. P. Alfeld, *Comput. Aided Geom. Design*, **1**, 169 (1984).

11. S. E. Stead, *Rocky Mountain J. Math.*, **14**, 265 (1984).

12. P. A. Whitlock, J. T. Muckerman, and E. R. Fisher, J. Chem. Phys., **76**, 4468 (1982).

13. D. G. Truhlar and J. T. Muckerman, Ch. 16 in Atom-Molecule Collision Theory: A Guide for the Experimentalist, R. B. Bernstein, Ed. Plenum Press, New York (1979).

14. Again, more sophisticated binning techniques could have been employed (see ref. 13), but, when alternatives were explored, little difference was observed. In particular, we used both the rotational energy $N(N+1)B = E_{rot}$ and the rotational angular momentum $\mu_{Zn\text{-}H'} \tau^2 \, d\Delta/dt = N \hbar$ to evaluate N, and we used the vibrational energy $\hbar \, (k/\mu_{Zn\text{-}H'})^{1/2} (v+1/2)$ and the action $S = \int \mu_{Zn\text{-}H'} (d\tau/dt) \, d\tau = (v+1/2) \, h$ to compute v.

Table I. Predicted L_z values for four isotopic cases showing isotope mass dependence.

Isotopic Case	L_z (1/2,1/3,2/3) $\mu_{Zn,H/D}\,\mu^{-3/4}_{HH/DD/HD}$	Numerical Value[a] of L_z
ZnH from H_2	$1/2\ (1)\ (2)^{3/4}=0.84$	$13\hbar$
ZnH from HD	$2/3\ (1)\ (3/2)^{3/4}=0.90$	$14\hbar$
ZnD from D_2	$1/2\ (2)\ (1)^{3/4}=1.0$	$15\hbar$
ZnD from HD	$1/3\ (2)\ (3/2)^{3/4}=0.90$	$14\hbar$

a. Computed using $L_z = \mu_{Zn,H/D}\,\tau\,v_{H/D}\sin\chi$ with the velocity obtained from the release of zero-point vibrational energy.

O
P(N)

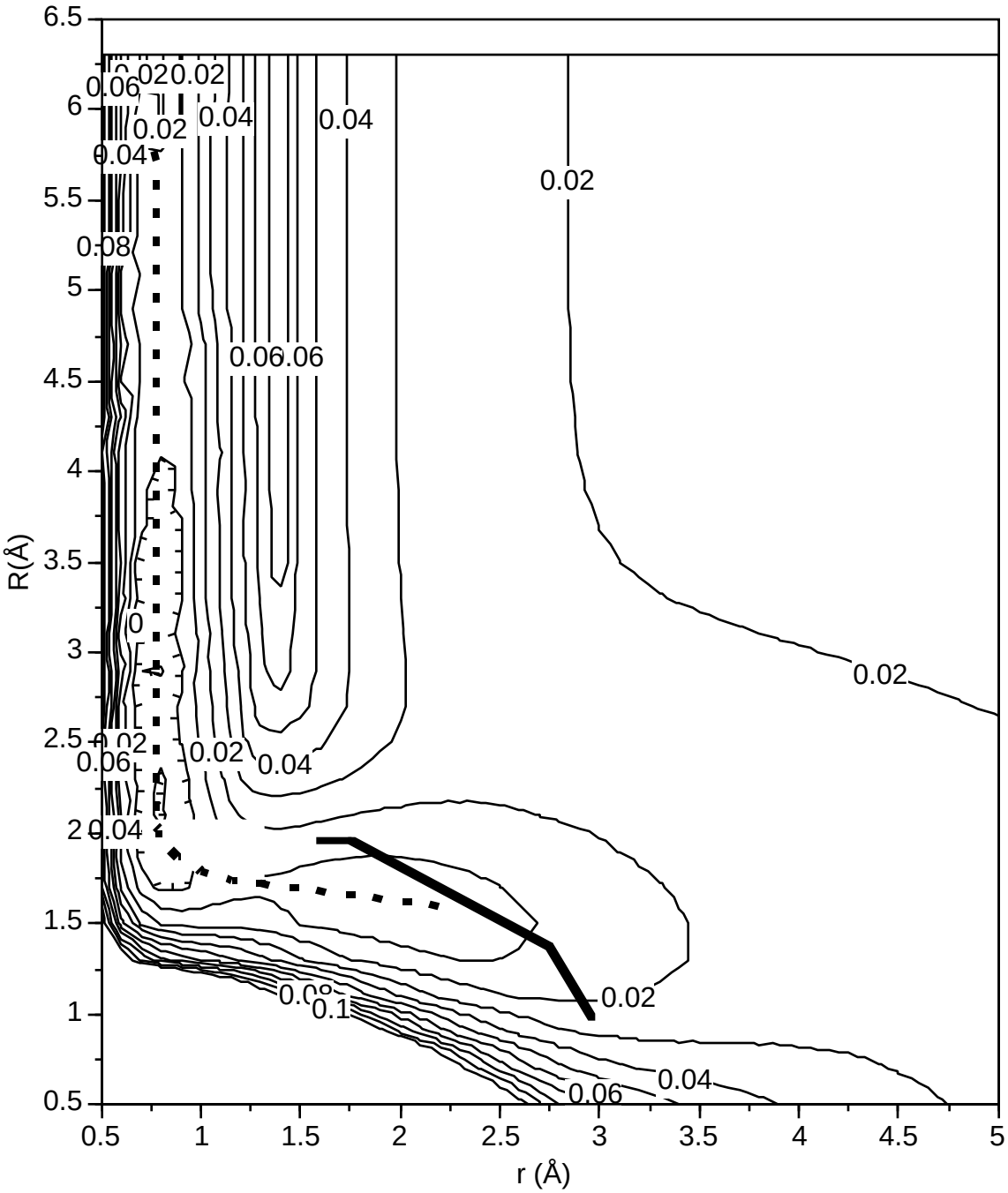
R(Å)
r (Å)
6.5
6
5.5
5
4.5
4
3.5
3
2.5
2
1.5
1
0.5
0.5
1
1.5
2
2.5
3
3.5
4
4.5
5
0.02
0.04
0.06
0.08
0.1

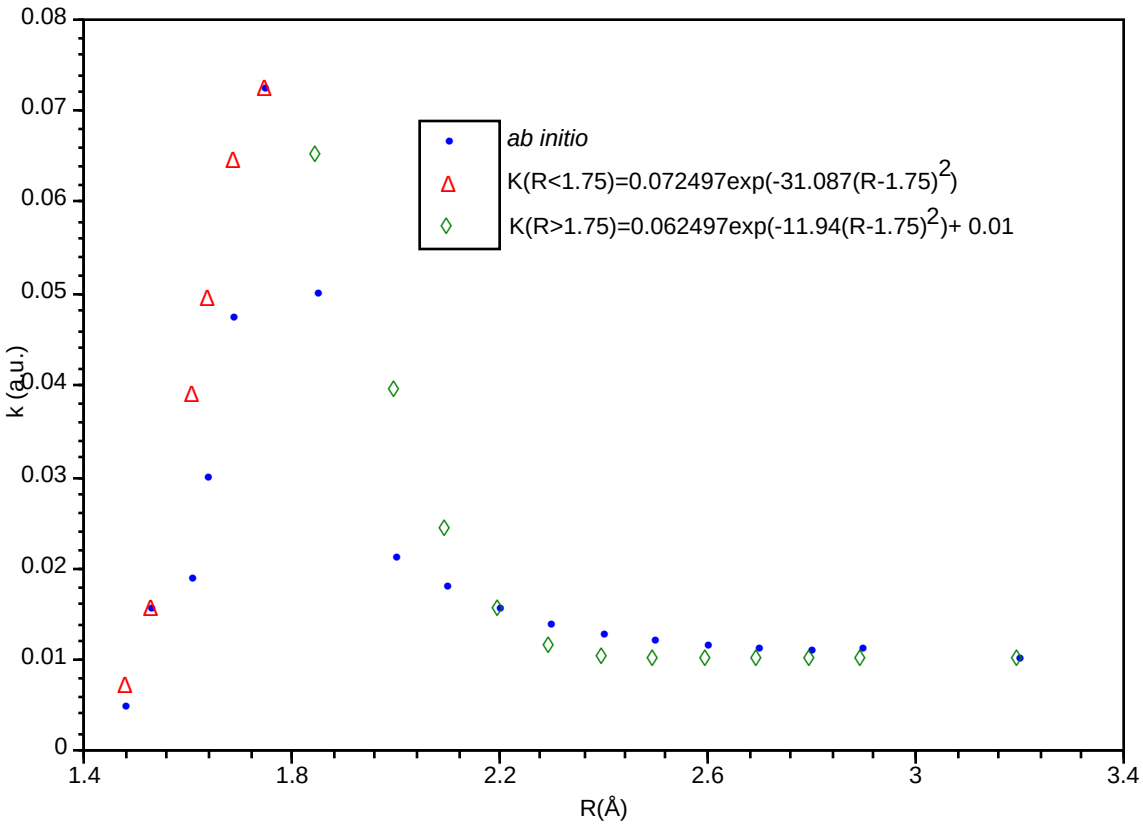
0.08
0.07
0.06
0.05
0.04
0.03
0.02
0.01
0
k (a.u.)
1.4
1.8
2.2
2.6
3
3.4
R(Å)
ab initio
K(R<1.75)=0.072497exp(-31.087(R-1.75)2)
K(R>1.75)=0.062497exp(-11.94(R-1.75)2)+ 0.01

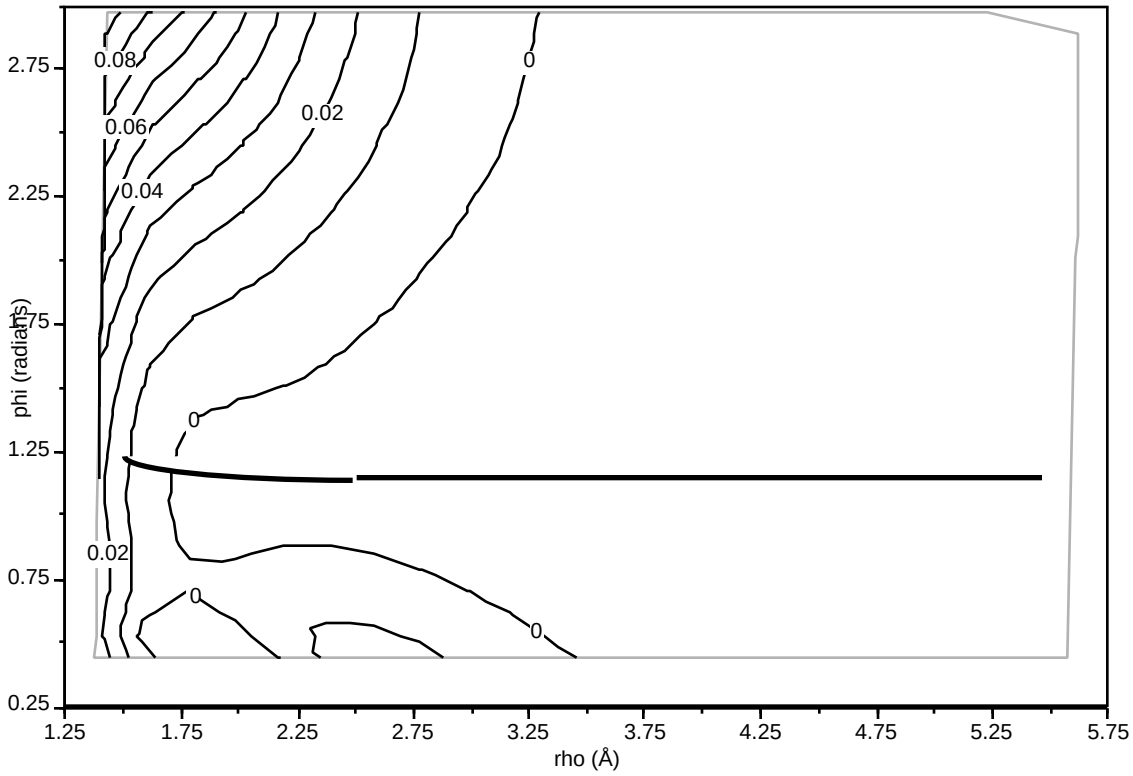
0.08
0.06
0.04
0.02
0
0.02
0
0
0
2.75
2.25
1.75
1.25
0.75
0.25
phi (radians)
1.25
1.75
2.25
2.75
3.25
3.75
4.25
4.75
5.25
5.75
rho (Å)

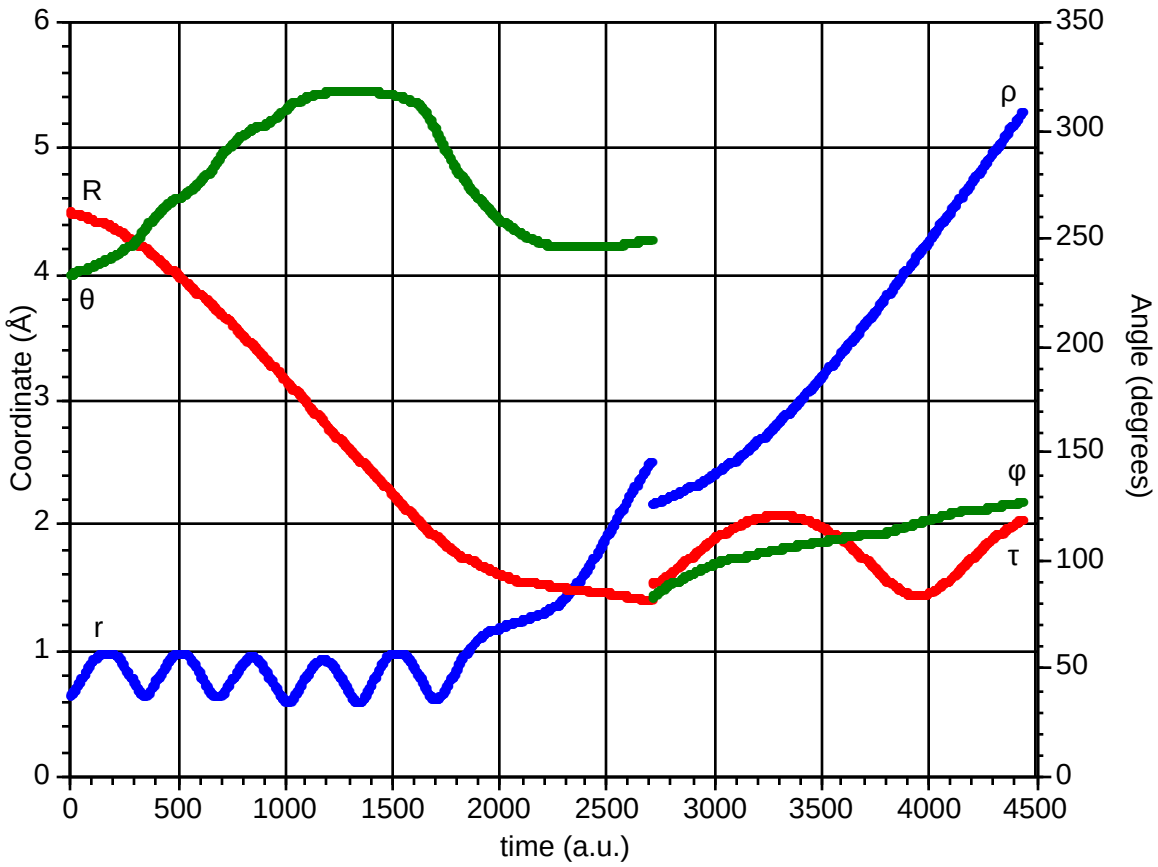
Coordinate (Å)
Angle (degrees)
time (a.u.)
R
θ
r
ρ
φ
τ
0
1
2
3
4
5
6
0
50
100
150
200
250
300
350
0
500
1000
1500
2000
2500
3000
3500
4000
4500

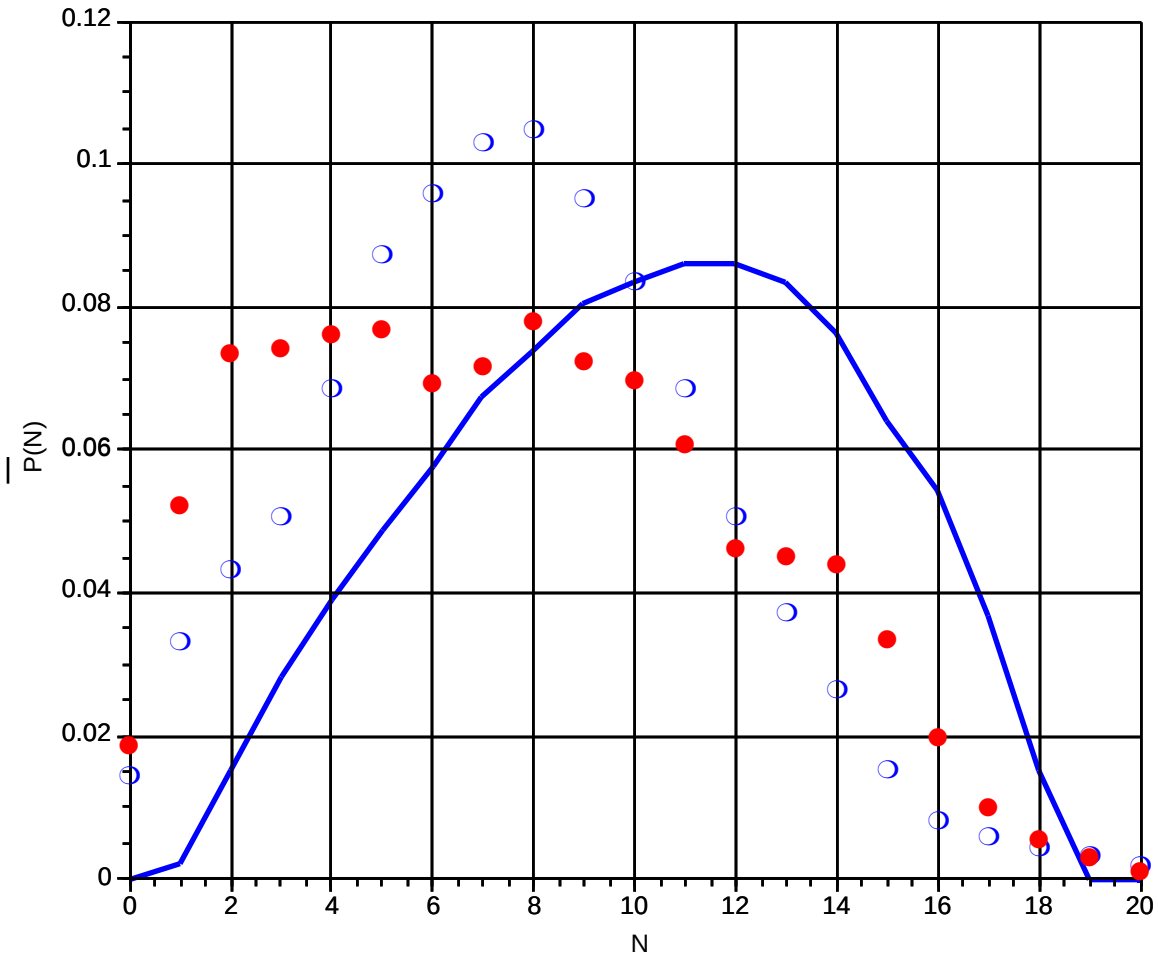
0.12
0.1
0.08
0.06
0.04
0.02
0
P(N)
0
2
4
6
8
10
12
14
16
18
20
N

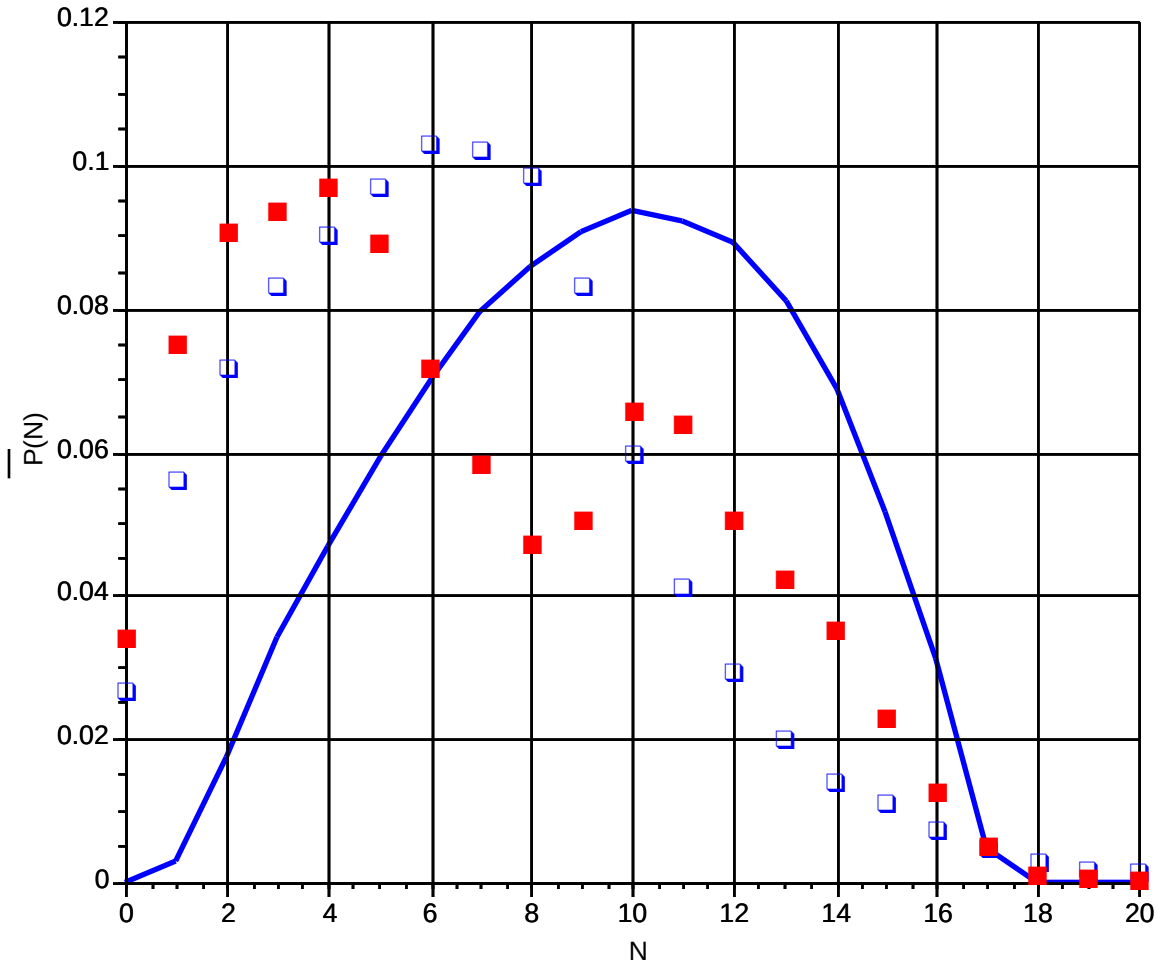
0.12
0.1
0.08
0.06
0.04
0.02
0
P(N)
0
2
4
6
8
10
12
14
16
18
20
N

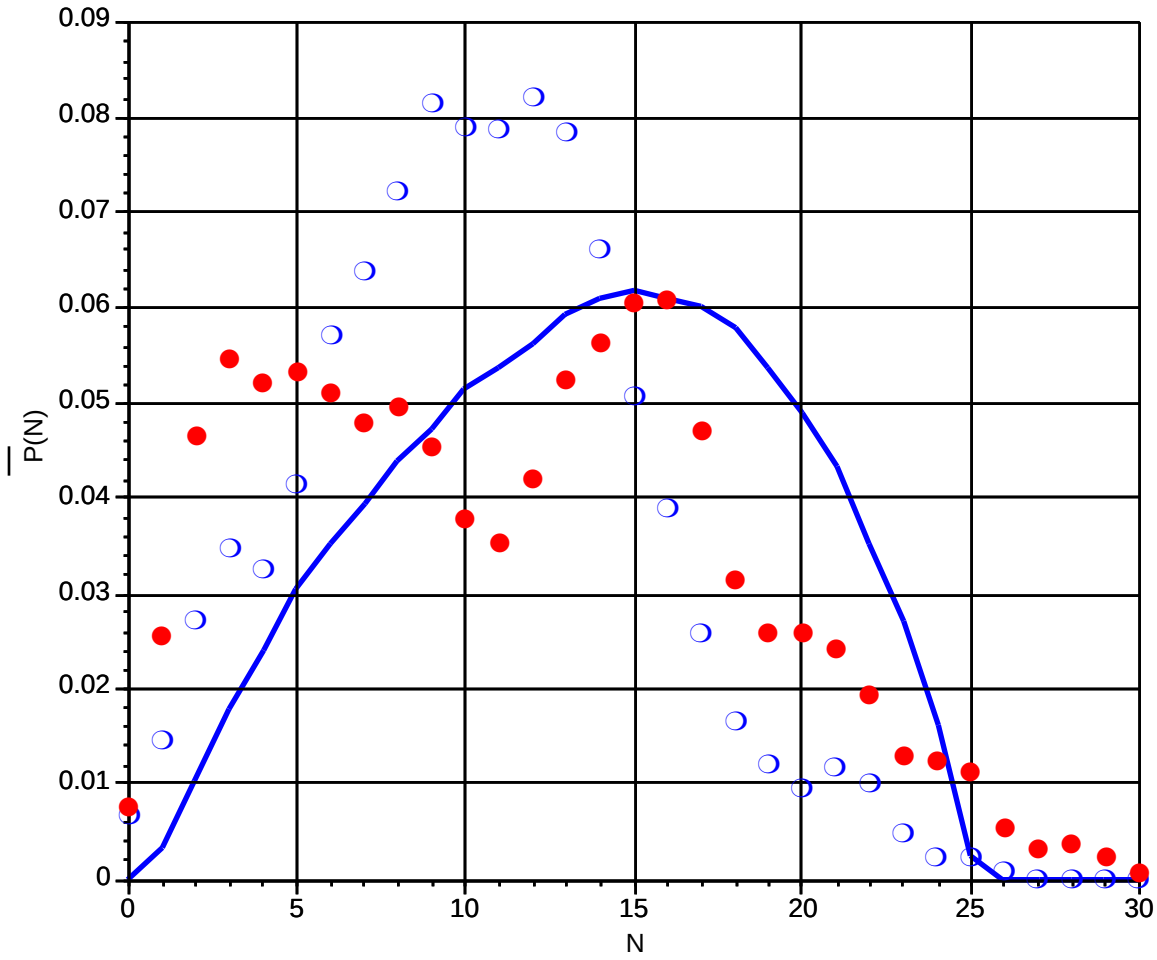
0.09
0.08
0.07
0.06
0.05
0.04
0.03
0.02
0.01
0
P(N)
0
5
10
15
20
25
30
N

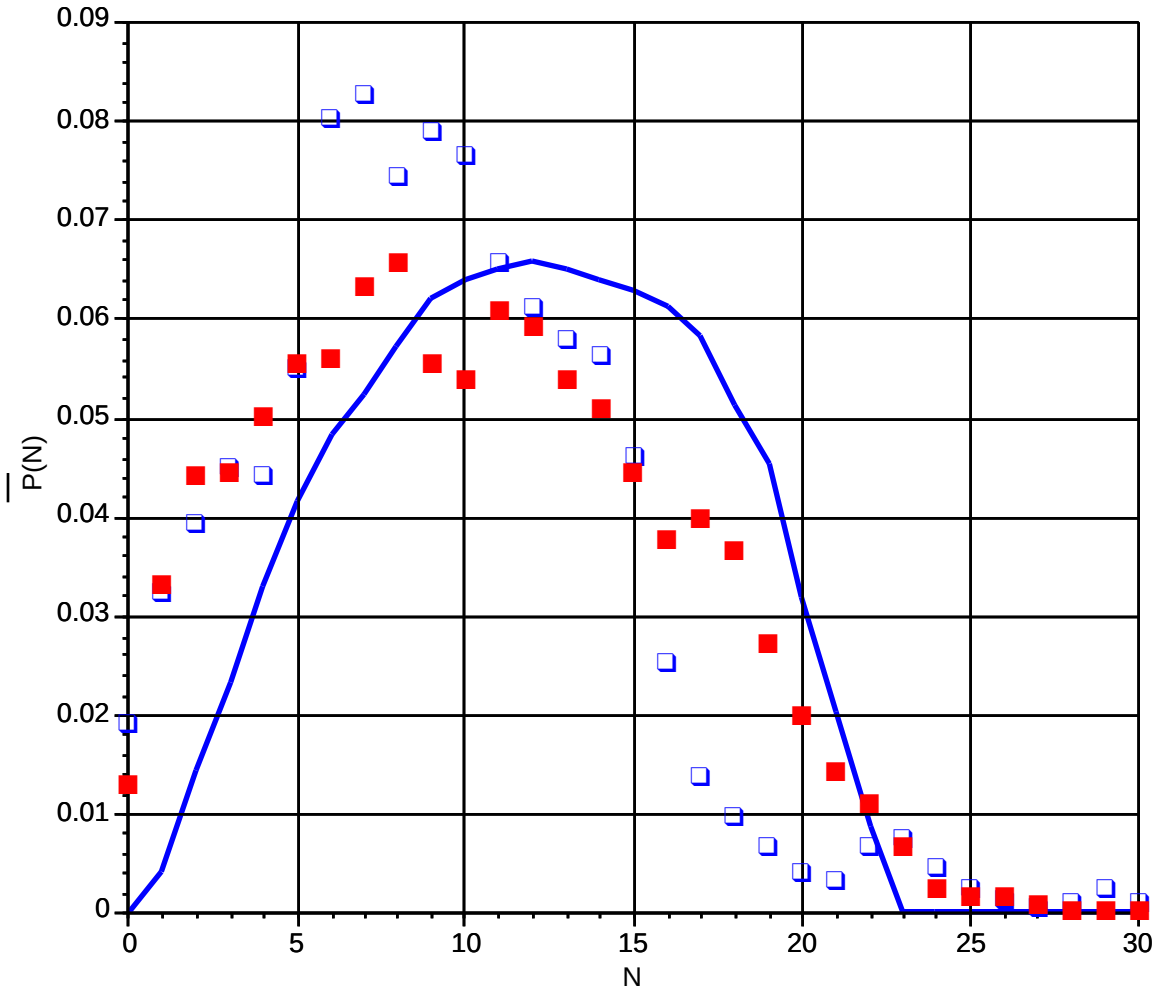
0.09
0.08
0.07
0.06
0.05
0.04
0.03
0.02
0.01
0
P(N)
0
5
10
15
20
25
30
N

$v_{H,per.}$ = component of v_H perpendicular to the nascent Zn-H bond axis

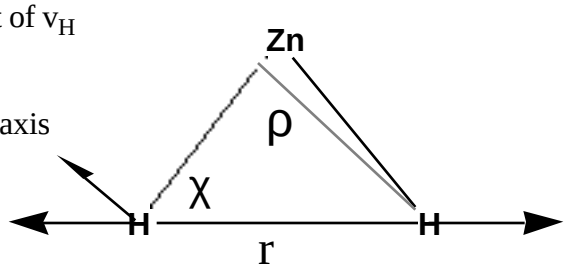

$$v_H = 1/2\ dr/dt$$

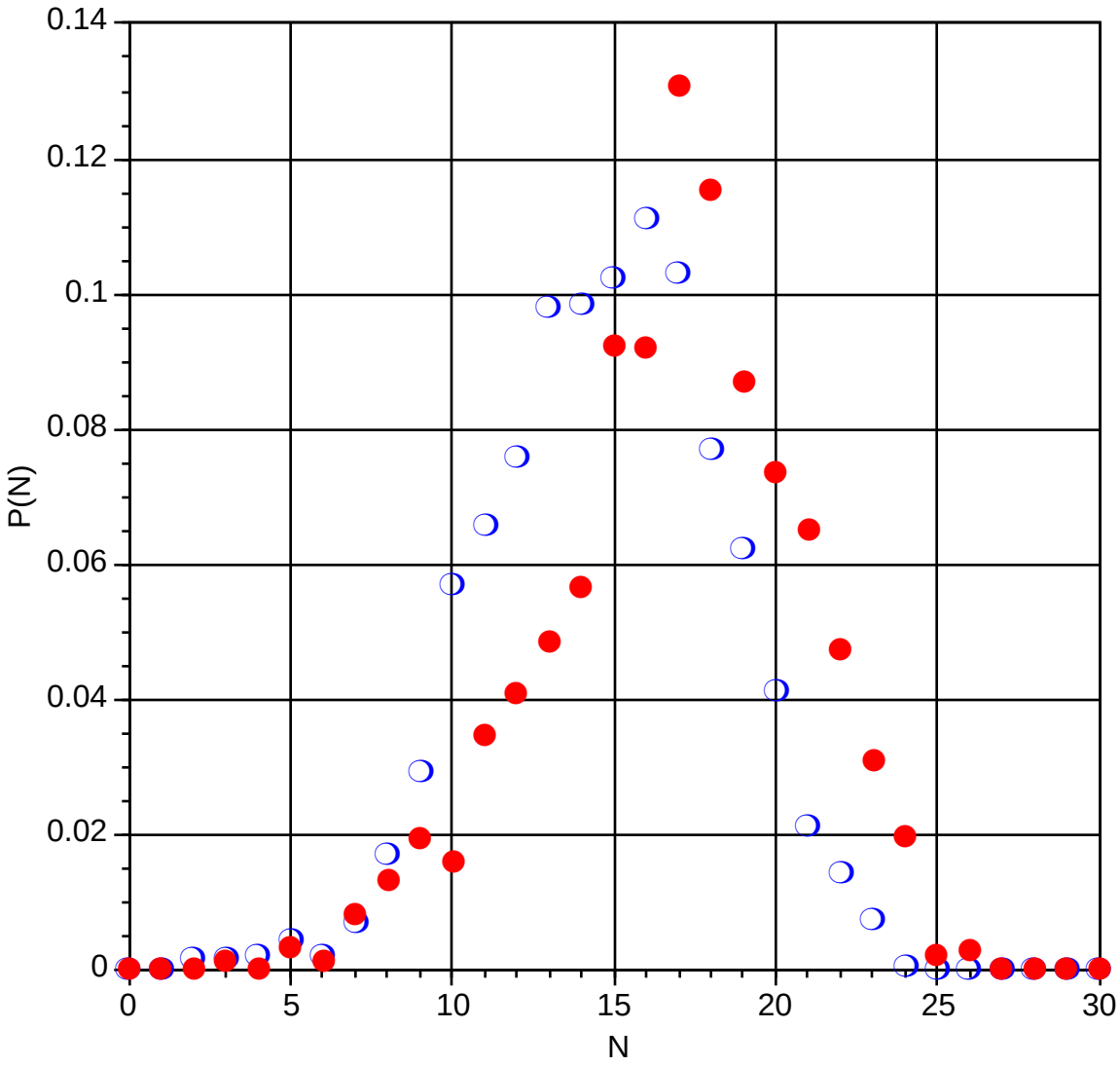
0.14
0.12
0.1
0.08
0.06
0.04
0.02
0
P(N)
0
5
10
15
20
25
30
N

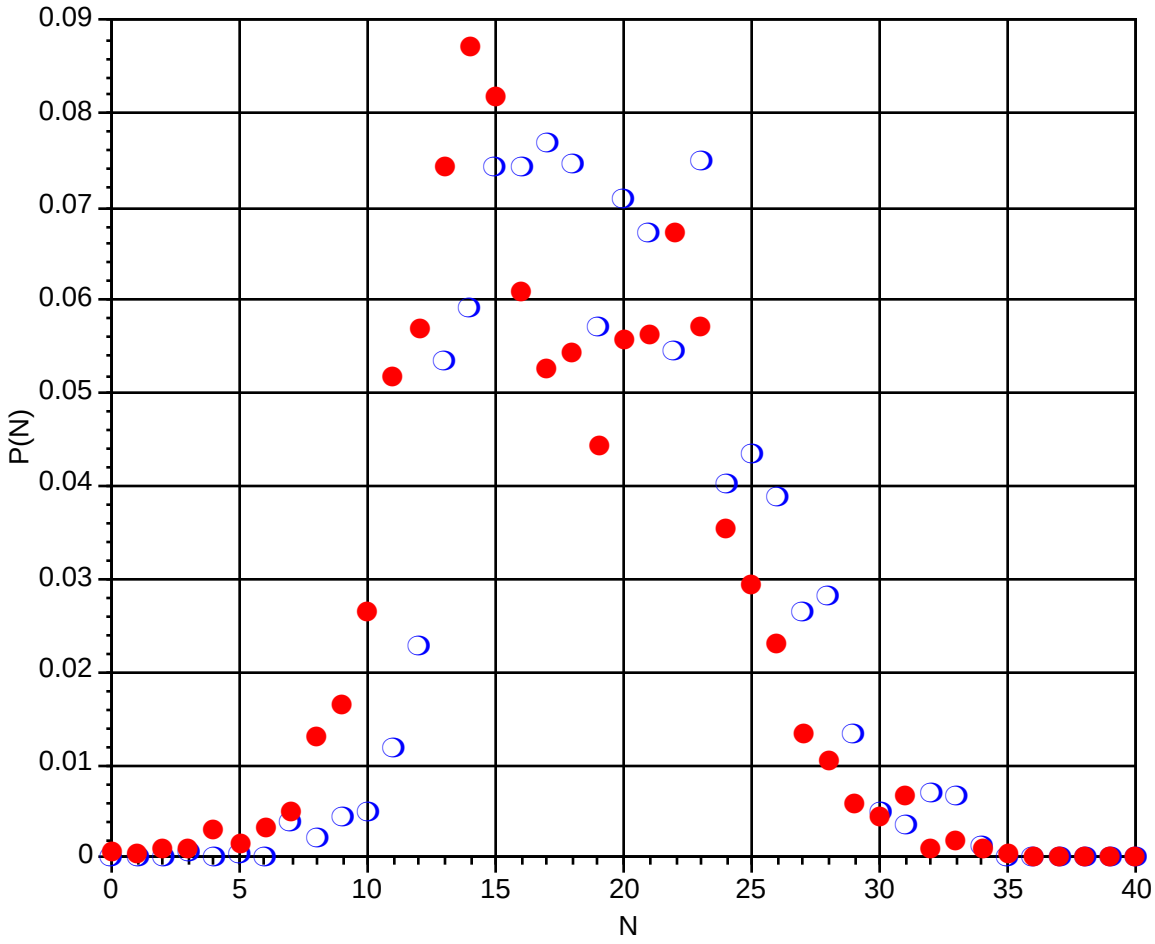
0.09
0.08
0.07
0.06
0.05
0.04
0.03
0.02
0.01
0
P(N)
0
5
10
15
20
25
30
35
40
N

Figure 1a. Product vibrational and rotational populations for ZnH produced from H_2 (open) and from HD (filled).

Figure 1b. Product vibrational and rotational populations for ZnD produced from D_2 (open) and from HD (filled).

Figure 2. Energy along the intrinsic reaction path of the scaled potential. The point S denotes the seam connecting the entrance- and exit-channels, and the mark near 0.2 eV on the energy axis shows the zero-point energy (plus the smallest collision energy considered) for the D_2 molecule; this is the minimum energy available in any reaction. The sketches at the bottom depict the molecular geometry at corresponding points along the IRC.

Figure 3. The asymmetric distortion force constant as a function of R along the IRC. The triangle function is used for R < 1.75 Å, and the open diamond function is used for R > 1.75 Å. The *ab initio* computed force constants are shown in dots.

Figure 4. Exit-channel energy surface for τ = 1.7Å. The contours are spaced by 0.01 Hartree (0.27 eV) and, again, the zero of energy is $Zn(^3P) + H_2$. The line is the IRC connecting to the seam on the entrance-channel and moving outward to ZnH + H products.

Figure 5. Plots of R, r, and θ vs time (in a.u.; 1.0 a.u. = 2.41889 x10^{-17} sec) up to the seam and then ρ, φ, and τ vs time.

Figure 6. Rotational populations for ZnH in v = 0 produced from H_2 (open circles) and from HD (filled circles). The solid line is our digitization of the experimental ZnH v=0 rotational distribution (from H_2 or from HD).

Figure 7. Rotational populations for ZnH in v = 1 produced from H_2 (open boxes) and from HD (filled boxes). The solid line is our digitization of the experimental ZnH v=1 rotational distribution (from H_2 or from HD).

Figure 8. Rotational populations for ZnD in v = 0 produced from D_2 (open circles) and from HD (filled circles). The solid line is our digitization of the experimental ZnD v=0 rotational distribution (from D_2 or from HD).

Figure 9. Rotational populations for ZnD in v = 1 produced from D_2 (open boxes) and from HD (filled boxes). The solid line is our digitization of the experimental ZnD v=1 rotational distribution (from D_2 or from HD).

Figure 10. Collision complex as it crosses the seam with large dr/dt (designated by the velocity arrows on the two separating H atoms, each having velocity $\frac{1}{2}\frac{dr}{dt}$). ρ is the Jacobi coordinate of the exit-channel, the distance from the departing H atom to the center of mass of the nascent ZnH.

Figure 11. Rotational populations for ZnH produced from H_2 (open circles) and from HD (filled circles) in the seam region.

Figure 12. Rotational populations for ZnD produced from D_2 (open circles) and from HD (filled circles) in the seam region.